HIGH CONTENT ANALYSIS OF HUNTINGTIN PHOSPHO-N17

HIGH CONTENT ANALYSIS TO IDENTIFY MODULATORS OF HUNTINGTIN N17 PHOSPHORYLATION

By REBECCA KURTZ, B.Sc. (Honours)

A Thesis Submitted to the School of Graduate Studies in Partial Fulfillment
Of the Requirements for the Degree Master of Science

McMaster University MASTER OF SCIENCE (2019)
Hamilton, Ontario
(Biochemistry and Biomedical Sciences)

TITLE: High Content Analysis to Identify Modifiers of Huntingtin N17 Phosphorylation
AUTHOR: Rebecca Kurtz,B.Sc. (Queen's University)
SUPERVISOR: Dr. Ray Truant
NUMBER OF PAGES: 45

Abstract

The N17 domain in the huntingtin protein is an important modulator of mutant huntingtin toxicity in Huntington's Disease (HD). Notably, this domain is hypophosphorylated in HD, and promoting its phosphorylation is protective in HD models. I conducted high content analysis of a library of 1163 compounds to identify modulators of phospho-N17 in order to gain mechanistic insight into the pathways which affect N17 phosphorylation. I found that the pharmaceutical compound Pranlukast promoted N17 phosphorylation by inhibiting the NFκB signaling pathway, which was also shown to modulate N17 phosphorylation in our lab's previous work. Throughout the course of this project, I developed a novel method for screening moderately sized compound libraries that is inexpensive, unbiased, sensitive, and accurate. This new high content analysis procedure, known as the "Gladiator" screening method, can be used as a framework to screen compounds in small laboratory.

Acknowledgments

I would like to thank my supervisor, Dr. Ray Truant for the support and knowledge you have provided me throughout the course of my studies. I would also like to thank my committee members, Dr. Sara Andres and Dr. Matthew Miller for all of their invaluable feedback and insights.

Thank you to Maria Maqsood, Jasmeet Singh, and William Pidduck for their contributions to this project. The Gladiator screen was a group effort and I am glad I had these three undergraduate students to share this project with.

Thank you to all the lab members who have taught me so much and helped me with my experiments and presentations. Dr. Tamara Maiuri, Dr. Laura Bowie, Dr. Claudia Hung, Mina Flacone, and Celeste Suart, thank you all!

Finally, thank you Mom, Dad, and Wilma for your love and support.

Table of Contents

Figure List

Abbreviations

ANOVA	Analysis of variance
ADP	Adenosine diphosphate
APRT	adenine phosphoribosyltransferase
ASO	antisense oligonucleotide
ATM	Ataxia-telangiectasia mutated
ATP	Adenosine triphosphate
CAA	Cytosine-adenine- adenine
CAG	Cytosine-adenine-guanine
CK2	Casein kinase-2
CRM1	chromosome region maintenance-1
DMSO	Dimethyl sulfoxide
DNA	Deoxyribonucleic acid
FAN1	Fanconi anemia FANCD2- and FANCI-associated nuclease 1
FDA	Food and Drug Administration
FBS	fetal bovine serum
FLIM-FRET	Fluorescence Lifetime Imaging- Förster resonance energy transfer
GDP	Guanosine diphosphate
GTP	Guanosine triphosphate
GWAS	Genome Wide Association Study
HD	Huntington's Disease
HEAT	Huntingtin, Elongation factor 3, Protein Phosphatases 2A, mTOR
HMGB1	High Mobility Group Box protein
HTT	Huntingtin
ICL	Interstrand Cross-Link
IKK	IκB kinase
IVS	intervening sequence
kDa	kilodalton
KTP	Kinetin triphosphate
MEM	minimal Eagle's medium
MMR	Mismatch repair
MMS	methyl methanesulfonate
N17	Alpha-helical domain of the huntingtin protein composed of the first 17 amino acid residues at the amino-terminal
N6FFA	N6-furfuryladenine
NFκB	nuclear factor kappa-light-chain-enhancer of activated B cells
NMR	Nuclear magnetic resonance
P-N17	Phosphorylated N17
PAR	Poly ADP-ribose
PBS	phosphate buffer saline
PCA	Principal component analysis
Phospho-N17	Phosphorylated N17
PRMT5	Protein Arginine Methyltransferase 5
PY-NLS	Proline-tyrosine nuclear localization signal
ROS	Reactive oxygen species

S13	Serine 13
S16	Serine 16
SAM	S-adenosyl methionine
SNP	Single nucleotide polymorphism

Declaration of Academic Achievement

All experimental content within this thesis is the work of the author, Rebecca Kurtz, except for the following:

Maria Maqsood, Jasmeet Singh, and William Pidduck helped with the 14 primary FDA compound screens (data not included) and the secondary screens in Figure 1B.

Chapter 1

Introduction

1.1 – Huntington's Disease

1.1.1 - Symptoms and Neuropathology

Huntington's Disease (HD) is an inherited age-onset neurodegenerative disease first described by American medical doctor George Huntington in 1872 as an inherited form of chorea, a neurological disorder characterized by involuntary dance-like movements (1). Along with motor dysfunction, HD patients also suffer from psychiatric symptoms and cognitive decline (2). HD patients have a life expectancy of 15 to 20 years after symptoms first appear (3). Most HD deaths occur as a result of difficulty swallowing (dysphagia) in the form of aspiration pneumonia (4,5). Cardiovascular disease is the second leading cause of HD deaths, followed by suicide (5).

HD is characterized by neuronal loss, most notably in the caudate nucleus and putamen in the striatum. Other areas of the brain, such as the cerebral cortex, thalamus, and the limbic system, are also affected as the disease progresses. (6).

1.1.2 - Genetics of HD

The pathogenesis of HD is due to an expansion of the CAG repeat tract in exon 1 of the HTT (huntingtin) gene, also known as IT15 (interesting transcript 15), located on the short arm of chromosome 4 (7). The expansion mutation, which results in additional glutamine repeats in the 350 kDa huntingtin protein, is inherited in an autosomal dominant manner. Therefore, the offspring of someone with HD has a 50% chance of inheriting the disease themselves.

HD patients have over 35 CAG repeats in the huntingtin gene while most people have 6-35 repeats (8). The repeat length is inversely correlated to the age of disease onset, as individuals with more repeat lengths tend to develop symptoms earlier than those with fewer repeats (8, 9). The disease is fully penetrant when the CAG repeat length is greater than 40 but is only partially penetrant with 36 to 40 repeats (9). However, the age of disease onset is highly variable even amongst individuals with the same number of glutamine repeats. CAG repeat length accounts for 50–70% of the variance in age of disease onset (10).

Long CAG tracts are unstable and are susceptible to expansion and, to a lesser extent, contraction. Expansion of the CAG tract occurs in the HD brain, resulting in the addition of up to hundreds of repeats in some areas (11, 12). Repeat lengths also tend to increase in size across successive generations in HD families resulting in earlier ages of onset, a phenomenon known as genetic anticipation, but only when inherited paternally (13-15). The difference between maternal and paternal inheritance on anticipation exists because expansion occurs during spermatogenesis but not oogenesis (16, 17).

1.1.3 - Age of Onset

The age of disease onset in HD can occur anytime between childhood and old age, but most typically occurs between the ages of 35-50 (3). While the number of CAG repeats in the huntingtin gene has the greatest influence on the age of disease onset, other factors that affect the age at onset at have recently been identified. An HD variant with an interrupting CAA codon

(which also codes for glutamine) at the penultimate position of the CAG tract is associated with an age of onset that is on average 25 years later than the variant without the interrupting adenosine that has the same number of repeats (18).

Genome wide association studies (GWAS) have found that SNPs in genes involved in DNA repair pathways and redox control are associated with HD age of onset (10, 19). Increased expression of interstrand cross-link (ICL) repair protein Fanconi anemia FANCD2- and FANCI-associated nuclease 1 (FAN1) correlates with a later age of onset. On the other hand, the expression of mismatch repair (MMR) proteins is associated with more somatic instability and earlier age of onset.

The GWAS data implicate DNA damage repair pathways as modifiers of HD age of onset, and Huntingtin's recent identification as a DNA damage repair protein part of the ATM complex (20) further strengthens the connection between DNA damage repair and the pathogenesis of HD.

1.2 - Huntingtin Protein

1.2.1 - Huntingtin Structure and Function

The 350 kDa huntingtin protein is expressed in all cell types where it is involved in several cellular processes, including endocytosis, vesicular trafficking, synaptic transmission, stress response, and DNA damage repair (20-22).

Huntingtin consists mainly of HEAT (Huntingtin, Elongation factor 3, Protein Phosphatases 2A, mTOR) repeats, which are 37-43 amino acid long motif consisting of two alpha helices connected by a loop (23). Several of these repeats together form a solenoidal protein that can act as a scaffold for protein-protein interactions, as was predicted for huntingtin (24-27). The cryo-electron microscopy structure solved in 2018 found that huntingtin contains two α-solenoidal HEAT-repeat domains, one the N-terminal domain and the other the C-terminal domain, linked by an unstructured, flexible bridge domain (28).

Exon 1 of the protein (residues 1-90) contains the N17 domain at the amino-terminal followed by the polyglutamine tract, and finally a polyproline tract at the carboxyl-terminal. The N17 domain, consisting of the first 17 amino acid residues, was predicted to form an amphipathic α-helix (29), which was confirmed with circular dichroism spectroscopy (29), x-ray crystallography (30), and NMR (31).

1.2.2 - Huntingtin Cellular Localization

In several cell types including neurons, huntingtin is primarily a cytoplasmic protein that is seen at the endoplasmic reticulum, Golgi, and vesicle membranes (32, 33), but can also translocate to the nucleus (34). In the cytoplasm, huntingtin binds the endoplasmic reticulum membrane as well as autophagic vesicles and late endosomes at the N17 domain, but can also translocate to the nucleus in response to changes in temperature (29) and oxidative stress (35). The oxidation of methionine residue 8 (M8) by the presence of ROS causes an increase in α-helical content in the

N17 domain and increases solubility from the endoplasmic reticulum membrane (35), exposing two serine residues, S13 and S16, which get phosphorylated by casein kinase-2 (CK2) (36).

The dissociation from the endoplasmic reticulum allows huntingtin to be actively transported to the nucleus via a karyopherin β1/β2-type proline-tyrosine nuclear localization signal (PY-NLS) located across residues 174-207 (37). Nuclear localization is also dependent upon High Mobility Group Box protein (HMGB1) binding to the intervening sequence (IVS) within the PY-NLS and well as N17 (38). At sites of oxidative damage in the nucleus, phosphorylated huntingtin co-localizes with ATM to chromatin-dependent nuclear puncta (20), later identified as nuclear speckles (39). Phospho-huntingtin also localizes to the centrosomes and, during cell division, the cell-cleavage furrow and tubulin spindle fibers (36).

Huntingtin's nuclear export is dependent on chromosome region maintenance-1 (CRM1) binding with GTP-coupled Ran to the highly conserved, leucine-rich nuclear export signal (NES) located on the N17 domain , as well as a Ran-GTP/Ran-GDP gradient across the nuclear membrane (34, 40, 41). When phosphorylated, the phosphate groups at S13 and S16 block CRM1 from binding to the NES, thereby preventing nuclear export. Once DNA damage has been repaired and oxidative stress has been relieved, phosphatases dephosphorylate both N17 serine residues, allowing for CRM1 binding and huntingtin's nuclear export.

1.3 - Mutant Huntingtin Dysregulation and Toxicity in HD

1.3.1 - Toxic Aggregate Theory

It was widely believed that aggregates of huntingtin fragments cause the neuronal loss in HD because long polyglutamine domains can form polar zipper interactions (42) and inclusions of huntingtin fragments are seen in the brains of HD mouse models (43) and post-mortem HD patient brains (44). However, current evidence indicates that inclusions are not the cause of HD pathogenesis but rather a downstream effect of huntingtin dysfunction in DNA damage repair and may even be a protective mechanism (45-47).

1.3.2 - Loss of Function in Oxidative DNA Damage Repair

DNA damage repair has been implicated in HD pathogenesis through both GWAS (10, 19) and our group's findings that huntingtin is involved in oxidative DNA damage repair (20, 48, 49). The buildup of oxidative damage due to insufficient DNA damage repair in HD likely contributes to neuronal death, and the age onset nature of this disease may be due to an inability to handle increasing ROS load in the brain as it ages. Furthermore, suboptimal DNA damage repair could be responsible for many hallmarks of HD, including the dysregulation of energy balance, huntingtin aggregates in the brain, and mitochondrial dysfunction (48, 49).

Energy balance in HD is dysregulated, with high ADP/ATP ratios in HD patient brains (50), as well as mouse model brains (51) and HD cell lines (39). The formation of PAR chains in response to unrepaired DNA damage could drain the cells of energy and leads to a further lack of repair (48). Huntingtin inclusions present in brains could be a consequence of energy depletion, since chaperones require ATP energy to prevent and correct protein aggregation (48).

Mitochondrial dysfunction, widely seen in HD (52), can be caused by DNA damage, and thus may also be a consequence of impaired DNA damage repair in HD.

Several long standing phenotypes of HD could be explained by mutant huntingtin's suboptimal function in DNA damage repair. The hypothesis that HD is caused by a lack of DNA repair is supported by the recent evidence that DNA damage repair and oxidative stress pathways play a role in the pathogenesis of HD.

1.3.3 - Mutant Huntingtin Gain-of-Function Toxicity

While the presence of insoluble, fibrillar inclusions of polyglutamine expanded huntingtin appear to be protective against neuronal death, globular inclusions in the nucleus that are capable of exchanging with the soluble phase are toxic (47). The phosphorylation status of serine residues S13 and S16 on the N17 domain seems to affect mutant huntingtin's toxicity. The toxic, globular inclusions contain unphosphorylated N17 huntingtin, while the protective, fibrillar inclusions are composed of phosphorylated N17 huntingtin (47). Polyglutamine expanded huntingtin is hypophosphorylated compared to wildtype huntingtin (36, 39), and N17 phosphorylation is protective in HD mouse models (53, 54) and cell culture models (36).

It is hypothesized that the polyglutamine tract in huntingtin normally acts as a hinge region, but loses its flexibility and adopts a toxic conformation when expanded beyond 35 repeats (55). FLIM-FRET experiments support the "rusty hinge hypothesis," and show that unphosphorylated N17 mutant huntingtin is less flexible in the polyglutamine tract compared to phosphorylated N17 mutant huntingtin and wildtype huntingtin (56).

The N17 helix and the polyglutamine region lose their secondary structure characteristics when the polyglutamine tract is expanded, and the loss is more severe with increasing repeat lengths. It is hypothesized that the N17 helix and the polyglutamine tract interact more with one another at higher repeat numbers, creating a disordered conformation (57, 58). Imprinting of the expanded polyglutamine tract against the N17 helix may reduce polyglutamine flexibility, hinder N17 phosphorylation by blocking CK2 access, and prevent nuclear export of huntingtin by blocking CRM1 binding (34). The hypophosphorylation of N17 in HD may also be due in part to a lack of ATP required for CK2 activity. The typical midlife age of onset in HD could be explained by the increasing ROS levels in the aging brain driving more toxic mutant huntingtin into the nucleus.

Phosphate groups at S13 and S16 may prevent structural imprinting against the expanded polyglutamine tract, and thus inducing N17 phosphorylation could help mutant huntingtin maintain its flexible conformation and allow for the CRM1-facilitated nuclear export of huntingtin following dephosphorylation.

1.4 - Emerging HD Therapeutics

1.4.1 - N6-furfuryladenine

The observed protective effect of N17 phosphorylation led our group to conduct a high content screen of natural compounds. The cytokine N6-furfuryladenine, also known as N6FFA or

kinetin, was identified as a promoter of N17 phosphorylation (59). N6FFA was also protective in HD cell cultures and mouse models and reduced huntingtin inclusions in HD mouse brains, validating phospho-N17 as a therapeutic target in HD.

N6FFA is a natural by-product of oxidative DNA damage, formed by the addition of a furfuryl group to adenosine under Fenton-reaction conditions (60) and subsequent excision from the DNA backbone during DNA damage repair (61). N6FFA can be salvaged by the enzyme adenine phosphoribosyltransferase (APRT) and converted into kinetin triphosphate (KTP), an analog of ATP (62), which can be used by CK2 to phosphorylate N17 (59). Once again, oxidative DNA repair is implicated in HD with N6FFA.

While the lack of DNA damage repair in HD could be responsible for the lack of ATP needed to activate CK2, it could also result in decreased N6FFA levels and thus less KTP activation of CK2 and phosphorylation of N17. Treating with exogenous N6FFA appears to correct this phenotype by activating CK2, increasing N17 phosphorylation, and kick-starting DNA damage repair by phosphorylating other repair proteins (59).

1.4.2 - Antisense Oligonucleotides (ASOs)

Lowering huntingtin levels in HD patients with antisense oligonucleotides (ASOs) is currently a promising therapeutic treatment for HD. ASOs target and destroy messenger RNA for the huntingtin protein, thus reducing the overall amount of mutant huntingtin and its associated toxicity. In animal models, ASOs lower huntingtin concentrations and improves disease phenotypes (63).

The IONIS-HTT_{Rx} ASO, which targets both mutant and wildtype huntingtin expression, was shown to reduce mutant huntingtin concentrations in cerebral spinal fluid in a phase 1–2a trial (64). PRECISION-HD1 and 2 ASOs developed by WAVE Life Sciences target SNPs specific to mutant huntingtin found in two thirds of HD patients, and therefore only lowers levels of mutant huntingtin (65). While their therapeutic efficacy and long term effects in patients are unknown, ASOs have the potential to prevent and treat the symptoms of HD.

Chapter 2

A Novel Method of High Content Analysis to Identify Modifiers of Huntingtin N17 Phosphorylation

2.1 - Project Overview

2.1.1 - Rational

The alpha helical N17 domain of huntingtin is critical to the protein's intracellular localization and function, and the phosphorylation of serine residues S13 and S16 plays an important role in the pathology of HD. N17 is hypophosphorylated in individuals with the disease and restoring phosphorylation is protective in cellular and animal HD models.

2.1.2 - Experimental research approach

Through the course of my project, I developed and validated a novel method for high content analysis that is inexpensive, sensitive, and unbiased. To gain insight into mechanisms by which N17 phosphorylation can be promoted, a library of 1163 FDA approved compounds was screened for the ability to modulate huntingtin phosphorylation. The diversity of the FDA library allowed for many cellular pathways to be targeted, and the depth of knowledge behind the compounds allowed for the meaningful interpretation of results.

The Gladiator screening process developed for this project involved screening a large compound library of 1163 FDA approved compounds, divided across 14 96-well plates, in multiple rounds followed by dose response analysis to validate hit compounds. The name was chosen because only the compounds with the greatest phenotypic effects on the cells move on to the next round of screening until only a few hit compounds remain. 14 separate primary screens were conducted for each of the 14 96-well plates of FDA compounds, and the selected hit compounds from each screen were then screened together in one of three secondary screens. The hit compounds from the secondary screens were then assayed for their ability to modulate phospho-N17 in dose response experiments.

2.2 - Results

2.2.1 - High-content "Gladiator" analysis identifies five compounds as promoters of N17 phosphorylation

1163 FDA compounds divided across 14 96-well plates were screened for their ability to modulate phosphorylated N17 huntingtin. TruHD-Q50Q40 cells (39) were treated with the compounds, followed by the primary conjugate anti–N17-S13pS16p antibody against N17 phosphorylated at the S13 and S16 residues (36). 12-bit depth images were taken automatically from multiple randomly selected locations in each well with the EVOS microscope (Thermo Fisher Scientific), images with interfering artifacts such as detritus and dying cells were deleted, and PCA (principal component analysis) plots were generated for each of the 14 plates using Phenoripper software (Fig. 1A).

Phenoripper software analyzes bitmap textural elements of cell images and plots the images as vectors in unitless, 3D space based on the three most variable textures using principal component analysis (PCA) (66). Points furthest away from each other on the plot represent images or groups

of images that are most dissimilar. This method of screening is both unbiased and highly sensitive, able to detect differences between image sets that are not detectable by the human eye.

Compounds which appeared furthest from the center of the PCA plots were selected as primary hits (Fig. 1A). These most obvious hit compounds were then deleted from the dataset and plots were regenerated to identify another round of hits on the outermost perimeter. Antiseptic and antibiotic compounds were disqualified as hits since we suspect that their impact on phospho-N17 is likely due to non-specific cellular stress. 129 compounds were identified as primary hits, 11.1% of the 1163 compounds in the library.

The 129 primary hit compounds were arranged into three new plates, each of which were screened at different methyl methanesulfonate (MMS) concentrations (Fig. 1B). MMS is alkylating agent that reliably and robustly induces DNA damage by methylating DNA at N7-deoxyguanosine and N3-deoxyadenosine. Testing the compounds after inducing damage to the DNA may provide a more accurate model system since DNA damage is implicated in the pathogenesis of HD and may also influence how the compounds affect the cells. The compounds that were hits in at least two out of the three MMS conditions were selected as secondary hits. With the secondary screen, the compounds were narrowed down to 20 secondary hits, 1.7% of the original 1163 compounds.

CellProfiler (67) was used to produce dose response curves for the 20 secondary hits by measuring the fluorescent intensity of the anti–N17-S13pS16p signal after cells were treated with different concentrations of the compounds. Five of the 20 secondary hits modulated phospho-N17 in a dose dependent manner, resulting in a final hit rate of 0.43%. Pranlukast, Clomipamine, Docetaxel, and Naftopidil increase N17 phosphorylation in a dose dependent manner with statistical significance, and Menadione also appears to promote N17 phosphorylation but lacks significance (Fig. 2A). The other 15 compounds, including Carbamazepine (Fig. 2A), did not result in a dose response and in some cases were toxic at high concentrations.

The Gladiator screen successfully identified five compounds (Pranlukast, Clomipamine, Docetaxel, Naftopidil and Menadione) out of 1163 that increase N17 phosphorylation in an unbiased manner (Fig. 3).

2.2.2 - Direct damage to DNA with intercalators does not affect N17 phosphorylation

Phosphorylated N17 huntingtin is recruited to sites of DNA damaged by irradiation (20), and thus we hypothesized that direct DNA damage promotes N17 phosphorylation. The five final hit compounds have flat heterocyclic structures, and thus could directly damage DNA by intercalating between base pairs. Cells were treated with known DNA intercalators ethidium bromide and Hoechst dye to test whether intercalation increases the phospho-N17 signal. CellProflier (67) was used to measure the phospho-N17 signal, and there was no significant difference between the fluorescence intensity of the treated and control cells (Fig 4).

2.2.3 - Pranlukast is the only cysteinyl leukotriene receptor antagonists that modulates N17 phosphorylation

Dose response experiments were conducted on Montelukast and Zafirlukast, both cysteinyl leukotriene receptor antagonists in the same family as the hit compound Pranlukast. Unlike Pranlukast, Montelukast and Zafirlukast did not increase N17 phosphorylation in a dose dependent fashion (Fig. 2B).

2.2.4 - Pranlukast inhibits NFκB

Pranlukast has been shown to inhibit the NFκB pathway (69-71), and inhibition of the NFκB pathway was previously shown by our lab to increase phospho-N17 (36). To confirm that Pranlukast inhibits NFκB, cells were treated with either Pranlukast, the IKK-2 and IKK-1 inhibitor BMS 345541 (Abcam) as a positive control, or vehicle control and then treated with the anti-NFκB p65 antibody [E379] (Abcam). Inhibition of NFκB results in cytoplasmic sequestration and increased degradation, and thus will result in lower levels of NFκB. CellProflier was used to measure the NFκB p65 fluorescence intensity. Pranlukast treated cells had lower NFκB p65 signals ($p<0.05$), as did the cells treated with BMS 345541 (not significant) (Fig. 5).

2.3 - Discussion

2.3.1 - Increasing phosphorylated N17 by generating oxidative stress

There was a possibility that direct DNA damage could increase phosphorylated N17, since phosphorylated N17 localizes to sites of DNA damage (20). Clomipramine, Docetaxel, Menadione, and Naftopidil may be capable of intercalating DNA due to their flat planar heterocyclic structures, which could explain their ability to increase phosphorylated N17. However, this does not appear to be the case, since known DNA intercalators ethidium bromide and Hoescht dye did not increase phosphorylated N17.

Oxidative stress induces phosphorylation of N17 (35), and thus I hypothesized that the final five hit compounds increase N17 phosphorylation by inducing oxidative stress. Clomipramine, Docetaxel, and Menadione have been reported to increase cellular ROS. Clomipramine is a tricyclic antidepressant drug that has been shown to increase levels of lipid peroxidases and hydroxyl radical production and decrease antioxidant protein activity (72). Docetaxel is taxane used to treat several types of cancer. Taxanes are mitochondrial poisons that induce the production of ROS (73). Menadione, a vitamin K supplement for animals, induces oxidative stress through redox cycling (74, 75), and was banned for human use by the FDA due to its toxicity. Naftopidil is a α1-adrenergic receptor antagonist (α1-blocker) that is approved for use in Japan to treat symptoms of benign prostatic hyperplasia. α-blockers, including Naftopidil, are not known to cause DNA damage or oxidative stress.

2.3.2 - Increasing phosphorylated N17 by inhibiting NFκB

Pranlukast is a cysteinyl leukotriene receptor antagonist that is used to treat bronchospasms caused by asthma or allergies. It is not used in the west, but is used in Asia, particularly in Japan. We determined that Pranlukast's ability to induce N17 phosphorylation is due to its inhibition of the NFκB signaling pathway. We have previously shown that inhibiting the NFκB pathway with

the IKKβ inhibitor BMS-345541 induces phosphorylation of N17 at serine residues S13 and S16 (36).

Cysteinyl leukotrienes can directly activate the NFκB pathway, and thus cysteinyl leukotrienes antagonists can inhibit NFκB signaling (68). However, Pranlukast can inhibit NFκB independently of its leukotriene antagonism (69-71). Neither Montelukast or Zafirlukast, cysteinyl leukotriene antagonists more potent that Pranlukast, increased N17 phosphorylation, which confirmed that Pranlukast's effect on N17 phosphorylation is not a result of its cysteinyl leukotriene antagonist activity. Pranlukast was shown to inhibit NFκB levels in cell culture.

The NFκB family of proteins are transcriptional activators activated by harmful cellular stimuli, such as oxidative stress, DNA damage, and proinflammatory cytokines. Genes that are targeted by NFκB usually promote cell survival, and thus are likely involved in attenuating toxic ROS levels. NFκB transcriptionally activates antioxidant proteins in many cell types, but can also target pro-oxidant genes in immune cells that generate ROS to defend against pathogens (76). It is likely that NFκB inhibition increases ROS in our system by decreasing the production of antioxidant proteins, thereby promoting N17 phosphorylation.

NFκB activation can promote both neuronal survival and death depending on how and where it is activated. NFκB activity in neurons is protective against oxidative stress-induced apoptosis due to the transcriptional activation of antioxidant proteins, particularly Mn-SOD, while NFκB activated by ischemic injury is harmful to neurons (77). The difference may be due to NFκB's activation in glial cells, since activated NFκB in microglia and astrocytes target pro-oxidant genes and promote neuronal death (78). Ischemic injury appears to activate NFκB in glial cells, which explains why inhibiting NFκB can be therapeutic in cases of acute brain and spinal cord injury. On the other hand, NFκB activated by oxidative and excitotoxic stress is protective against apoptosis due to its sole activation in neurons (79, 80). Therefore, due to high levels of ROS in HD brains that may be responsible for the diseases pathogenesis, NFκB inhibition is a poor therapeutic strategy for the treatment of HD.

2.3.3 - A novel method for high content analysis

I began my project with the goal to find compounds that induce N17 phosphorylation to gain insight on potential mechanisms of N17 phosphorylation. While I did have some success finding hit compounds that validate previous findings and support current hypotheses, I also developed and validated a novel method for high content analysis known as the "Gladiator" screen.

Out of 1163 compounds, I pulled out 15 compounds as potential hits, five of which were validated with dose response experiments. The screen was able to identify compounds that increased N17 phosphorylation with an accuracy of 25%. This method also resulted in an overall hit rate of 0.43%, which is considered good rate for a high content screen.

One of the hit compounds, Pranlukast, lead to the discovery that inhibition of the NFκB signaling pathways promotes N17 phosphorylation. This result also validates and explains our group's finding from 2011 that targeting the NFκB with IKKβ inhibition resulted in increased phospho-N17 (36).

This method can provide a framework for researchers to screen compound libraries in small laboratory settings in an efficient, inexpensive, unbiased and accurate way.

2.4 - Materials and Methods

2.4.1 - Tissue culture

TruHD-Q50Q40 patient derived fibroblasts expressing full length huntingtin were used because of their clinically relevant CAG repeat lengths and the hypophosphorylation of N17 phenotype (39). Cells were grown in minimal Eagle's medium (MEM) with 15% FBS and 1% Glutamax at 37°C and 5% CO_2 and 4% O_2.

2.4.2 - Antibodies

Previously characterized and validated polyclonal antibody against phosphorylated S13 and S16 of the N17 domain in huntingtin (anti–N17-S13pS16p) (35) was conjugated to Alexa Fluor 488 succinimidyl ester dye (Molecular Probes/Life Technologies) as previously described (57).

2.4.3 - FDA Compound treatment

Cells were seeded into 96-well plates, and once 80-90% confluent, were treated with a library of 1163 FDA approved compounds in DMSO for 6 hours at a concentration of 1 μM at 37°C and 5% CO_2 and 4% O_2 in 0.2% FBS MEM. For the secondary screens, the hit compounds from the primary screen were arranged into three 96-well plates, and each plate was screened under three conditions. Plates were treated with 40 or 80 μg/mL methyl methanesulfonate MMS in HBSS, or vehicle control, for 20 minutes at 37°C and 5% CO_2 and 4% O_2 prior to washing and treatment with the FDA compounds.

2.4.4 - Microscopy and image analysis

Images were acquired with the EVOS FL Auto 2 inverted widefield microscope (Thermofisher Scientific) at 20X magnification. For the high content analysis, several images were taken automatically per well from randomly selected locations.

Phenoripper software (66) analyzed the images in an unsupervised manner with a block size of 23 and generated PCA plots. Compounds that were furthest from the center of the PCA plot were selected as hit compounds.

2.4.5 - Dose Response Analysis

Cells were treated in triplicate with the compounds at 0.25, 0.5, 1, 2, 5, and in once case 10 μM concentrations for 6 hours in 0.2% FBS MEM at 37°C and 5% CO_2 and 4% O_2. Images were acquired with the EVOS FL 2 scope and analysed by CellProflier (67), which measured the relative fluorescence intensity of the phospho-N17 signal.

2.4.6 - Ethidium Bromide and Hoechst Treatment

Cells were treated in triplicate with 10 μg/ml ethidium bromide and Hoechst 33342 dye (Thermofisher Scientific) for 2 hours and 20 minutes respectively in triplicate, along with vehicle control wells. Images were acquired with the EVOS FL 2 scope and CellProfiler (67) measured the relative fluorescence intensity of the phospho-N17 signal.

2.4.7 - NFκB assay

Cells were treated in triplicate with either BMS-345541 (10μM), Pranlukast (5μM), or vehicle control for two hours in 15% FBS and 1% Glutamax at 37°C and 5% CO_2 and 4% O_2. Cells were treated with the anti-NFκB antibody and images were acquired with the EVOS microscope. CellProfiler (67) was used to measure the relative fluorescence intensity of the NFκB signal.

2.4.8 - Immunofluorescence

The cells were fixed and permeabilized with cold methanol for 10 min at -20°C, washed with phosphate buffer saline (PBS), and blocked for 1 hour in blocking buffer (2% FBS in PBS). Next, the cells were incubated with Alexa Fluor 488-conjugated anti–N17-S13pS16p primary antibody diluted 1:20 in antibody buffer (2% FBS and 0.02% TWEEN 20 in PBS) overnight at 4°C. Cells were then washed in PBS, treated with DRAQ5 nuclear stain (BioStatus) for 15 minutes, and washed again.

Cells treated with the anti-NFκB antibody were first fixed with 4% paraformaldehyde (PFA) for 15 minutes at room temperature, washed, and blocked in blocking buffer with 0.1% Triton X-100 to permeabilize for one hour. Cells were then incubated overnight with the validated polyclonal recombinant anti-NFκ-B p65 primary antibody [E379] (Abcam) diluted 1:100 at 4°C, washed, treated with goat anti rabbit Alexa Fluor 488 secondary antibody diluted 1:1000 for 30 minutes at room temperature, washed, and stained with DRAQ5.

Chapter 3

Huntingtin Lowering with Protein Arginine Methyltransferase 5 Inhibitors

3.1 - Project Overview

3.1.1 - Rational

Two Protein Arginine Methyltransferase 5 (PRMT5) inhibitors, LLY-283 and GSK-591, were shown to knock down total huntingtin levels in cell cultures, potentially as a result of epigenetic modification (data not shown). Huntingtin lowering with antisense oligonucleotides have shown efficacy in improving HD symptoms in HD animal models (63), and are now a promising therapeutic strategy for HD patients (64, 65). Therefore, the ability of these compounds to lower huntingtin levels could be of interest in HD research as a potential treatment.

3.1.2 - Background

PRMT5 is an enzyme that adds a methyl group from the cofactor S-adenosyl methionine (SAM) onto certain proteins, including histones, transcriptional elongation factors and p53. Histone methylation is an epigenetic modifier that can result in transcriptional silencing or promotion. PRMT5 methylates histones H3R8 and H4R3, which has been shown to repress the expression of tumor suppressor and cell cycle genes and promote hyperproliferation, while PRMT5 suppression results in slow growing cells (81). In the cytoplasm, PRMT5 is a part of the 20S methylosome complex, which methylates Sm proteins to form snRNPs that participate in RNA splicing (82).

LLY-283 and GSK-591 are PRMT5 inhibitors that have shown efficacy in treating secondary brain tumors and are currently being researched for cancer treatment in humans. LLY-283 is a small molecule with antitumor activity in xenograft mice that binds to the SAM pocket and competitively inhibits PRMT5 (82). GSK-591 is a peptide-competitive PRMT5 inhibitor that is also anti-tumorigenic and decreases the levels of SmBB′-Rme2s with similar potency to LLY-283 (82, 83).

3.1.3 - Experimental research approach

I investigated LLY-283 and GSK-591 for their effect on our cell culture system. I used immunofluorescence microscopy and unsupervised machine sorting with Phenoripper to detect phenotypic changes in the cells across different channels. I also conducted time response experiments measuring huntingtin levels to determine if the compounds lowered huntingtin over time in TruHD-Q50Q40 cells.

3.2 - Results

3.2.1 - Unsupervised machine sorting recognized phenotypic differences between PRMT5 inhibitor-treated cells

TruHD-Q50Q40 cells (39) were treated with PRMT5 inhibitors GSK-591 and LLY283, along with the inactive analogs, SGC-2096 and LLY-284, and a DMSO control at 1μM for 24 hours. Cells were treated with anti–N17-S13pS16p antibody, E7 anti-beta tubulin antibody, anti-huntingtin MAB2166, and nuclear stain DRAQ5. The EVOS microscope was used to take

multiple images of each treatment condition. PCA plots were generated with Phenoripper software (66) across each individual channel (Fig. 6).

Some separation between treatments was observed on the PCA plot of cells treated with the anti-huntingtin antibody (Fig. 6A). The cells treated with the active and control compounds all appear to be flattened compared to the DMSO control (Fig. 6E). Treatment of cells with the anti-beta tubulin antibody resulted clear separation between wells on the PCA plot (Fig. 6B). The GSK-591 and LLY-283 treated cells formed two distinct clusters separate from the control wells on the PCA plot of anti-P17 antibody treated cells (Fig. 6C), and both cell populations appear to be dimmer than cells treated with control compounds (Fig. 6E). The PCA plot of the DRAQ5 images showed separation between wells with the exception of GSK-591, which did not form a distinct cluster (Fig. 6D).

Unsupervised machine sorting with Phenoripper was able to detect phenotypic changes in cells treated with PRMT5 inhibitors within 24 hours, likely before huntingtin levels would be affected through epigenetic modification.

3.2.2 - Time Response of PRMT5 inhibitors

Cells were treated with GSK-591, SGC-2096 (neg. control), LLY283, LLY-284 (neg. control), or DMSO (vehicle control) for 1, 2, 3, or 4 days at 1μM. EPR-5526 anti-huntingtin antibody was used to quantify huntingtin levels through Western blot analysis. Due to time constraints, only one trial was conducted for each of the compounds.

Neither inactive compound, SGC-2096 and LLY-284, nor the active compound GSK-591 appeared to reduce huntingtin levels compared to untreated cells at any time point (Fig. 7). Active compound LLY-283 appeared to reduce huntingtin only after 4 days of treatment (Fig. 7).

3.3 - Discussion

GSK-591 and LLY-283 are equally potent at reducing methylation activity (82, 83), and yet their effects on cellular morphology in our system were distinct from one another. The separation by PCA of the DRAQ5 stained cells indicates that the compounds are affecting chromatin as would be expected with epigenetic modifiers. The morphological changes seen in the other channels may in part be due to PRMT5 inhibition, however, the inactive controls also changed the cells relative to a DMSO control. While PRMT5 inhibitors were intended to be used for epigenetic modification, the flattening of the cells observed indicates that the cytoskeleton is being affected by the small molecules. It is also unlikely that epigenetic modification would work to lower huntingtin within only 24 hours, so it is likely that the compounds are having off-target effects on cell morphology.

LLY-283 appeared to lower huntingtin levels only after 4 days of treatment, however, more replicates would need to be done to assure reproducibility and to determine if the effects are significant. GSK-591, on the other hand, did not appear to affect huntingtin expression. While PRMT5 inhibitors, particularly LLY-283, might be able to reduce huntingtin levels, it appears that they also have other off-target effects on cell morphology detected by unsupervised machine

sorting. The flattening of the treated cells could be indicative of toxicity. Even the inactive compounds with similar structures to the active compounds affected the cells phenotypically. Based on these results, GSK-591 and LLY-283 do not seem to be appropriate for HD treatment, despite their potential ability to lower huntingtin.

Unsupervised machine sorting by Phenoripper was able to unbiasedly detect phenotypic changes made by adding PRMT5 inhibitors and control compounds to the cultured cells in only one day. The methodology is highly sensitive, showing clear separation between images of the different cell populations using several fluorescent probes. Inhibiting PRMT5 may turn out to be a poor strategy for treating HD. However, unbiased machine learning with principal component analysis has confirmed with a high degree of sensitivity that the compounds affect cells phenotypically in ways distinct from one another. This software has the potential to be a useful tool in assessing the activity and efficacy of pharmaceutical compounds.

3.4 - Materials and Methods

3.4.1 - PRMT5 inhibitor treatment

For Phenoripper analysis, TruHD Q50Q40 cells (39) were seeded into 6-well plates. Once 80-90% confluent, were treated with 1μM of LLY-283, LLY-284, GSK-591, SGC-2096, (Structural Genomics Consortium) or DMSO in minimal Eagle's medium (MEM) with 15% FBS and 1% Glutamax for 24 hours at 37°C, 5% CO_2 and 4% O_2.

For Western blot analysis, cells were grown in 10cm plates and treated with 1μM of the compounds for 1, 2, 3, or 4 days in 15% FBS and 1% Glutamax at 37°C, 5% CO_2 and 4% O_2. Some cells were also treated with 1 μM DMSO for 24 hours.

3.4.2 - Immunofluorescence

Cells were fixed with cold methanol for 10 minutes at -20°C, blocked with 0.2% FBS for one hour and incubated with Alexa Fluor 488 conjugated rabbit anti–N17-S13pS16p primary antibody diluted 1:20 in antibody buffer (2% FBS and 0.02% TWEEN 20 in PBS) overnight at 4°C. The following day, cells were washed and treated with either mouse anti-beta tubulin primary antibody (E7, DSHB) or mouse anti-huntingtin MAB2166 antibody (Millipore) diluted 1:500 in antibody buffer, and incubated overnight. Then goat-anti-mouse Alexa Fluor 594 secondary antibody was diluted 1:500 in antibody buffer and added to the cells for 30 minutes. After washing, nuclei were stained with DRAQ5 (BioStatus) for 15 minutes, followed by washes.

3.4.3 - Unsupervised machine sorting

Multiple images were obtained by the EVOS microscope at 20X magnification from each treatment condition. Phenoripper software (66) was used to generate PCA plots across four different channels (MAB2166, beta-tubulin, P-N17, and DRAQ5).

3.4.4 - Western blot analysis

Media was aspirated out of the tissue culture plates over ice. Plates were then rinsed with PBS and aspirated thoroughly. Cells were lysed with 200 µl of RIPA buffer with 10% phosphatase and protease inhibitors (Roche), scraped from the plates, collected, and centrifuged at 10,000 × g for 10 minutes. The supernatants were collected and protein concentration was normalized.

30 µg of protein was loaded into pre-cast 4-20% polyacrylamide gradient gels (Biorad) for SDS-PAGE, and electroblotted onto Immobilin polyvinylidene difluoride (PVDF) membrane (EMD Millipore). Membranes were blocked in 5% non-fat dry milk in TBS-T (50 mM Tris-HCl, pH 7.5, 150 mM NaCl, 0.1% Tween-20) for 1 hour at room temperature or overnight at 4°C, then cut horizontally at 75-kDa to separate the huntingtin from the GAPDH. Membranes were treated with either rabbit EPR5526 (Abcam) diluted 1:2500 or mouse anti-GAPDH diluted 1:75,000 (Abcam) overnight at 4°C. Blots were washed with TBS-T, treated with anti-rabbit or anti-mouse horseradish peroxidase (HRP) secondary antibodies (Abcam) diluted 1:15,000 for 30 minutes at room temperature, and washed again.

Huntingtin bands were treated with enhanced chemiluminescent HRP substrate (EMD Millipore) and GAPDH bands were treated with Amersham ECL Western blotting detection reagent (General Electric Life Sciences). The blots were visualized on a MicroChemi system (DNR Bio-imaging Systems). Huntingtin bands were quantified using ImageJ (National Institutes of Health) and normalized to the GAPDH loading control.

Chapter 4

Conclusion

Huntingtin's N17 domain is a key modifier of mutant huntingtin toxicity in Huntington's Disease. Its phosphorylation at serine residues S13 and S16 is protective in HD, where it is hypophosphorylated compared to wildtype huntingtin. A high content analysis of an FDA compound library yielded five compounds that induce N17 phosphorylation, many of which induce oxidative stress, a known trigger for N17 phosphorylation. The compound Pranlukast is an inhibitor of the NFκB signaling pathway, the inhibition of which was previously shown by our lab in increase N17 phosphorylation.

The novel "Gladiator" screening method I developed identified compounds in an unbiased manner that target pathways known to affect N17 phosphorylation, validating it as an accurate tool. This is an accurate, unbiased, and inexpensive method of high content analysis that can be used by other labs to screen other libraries for other purposes.

Phenoripper software also proved to be useful in detecting phenotypic differences in cells treated by PRMT5 inhibitors in a short amount of time. Its accuracy, sensitivity, and the amount of images it can sort make unsupervised machine sorting an invaluable tool in pharmaceutical research and chemical biology.

Chapter 5

Figures

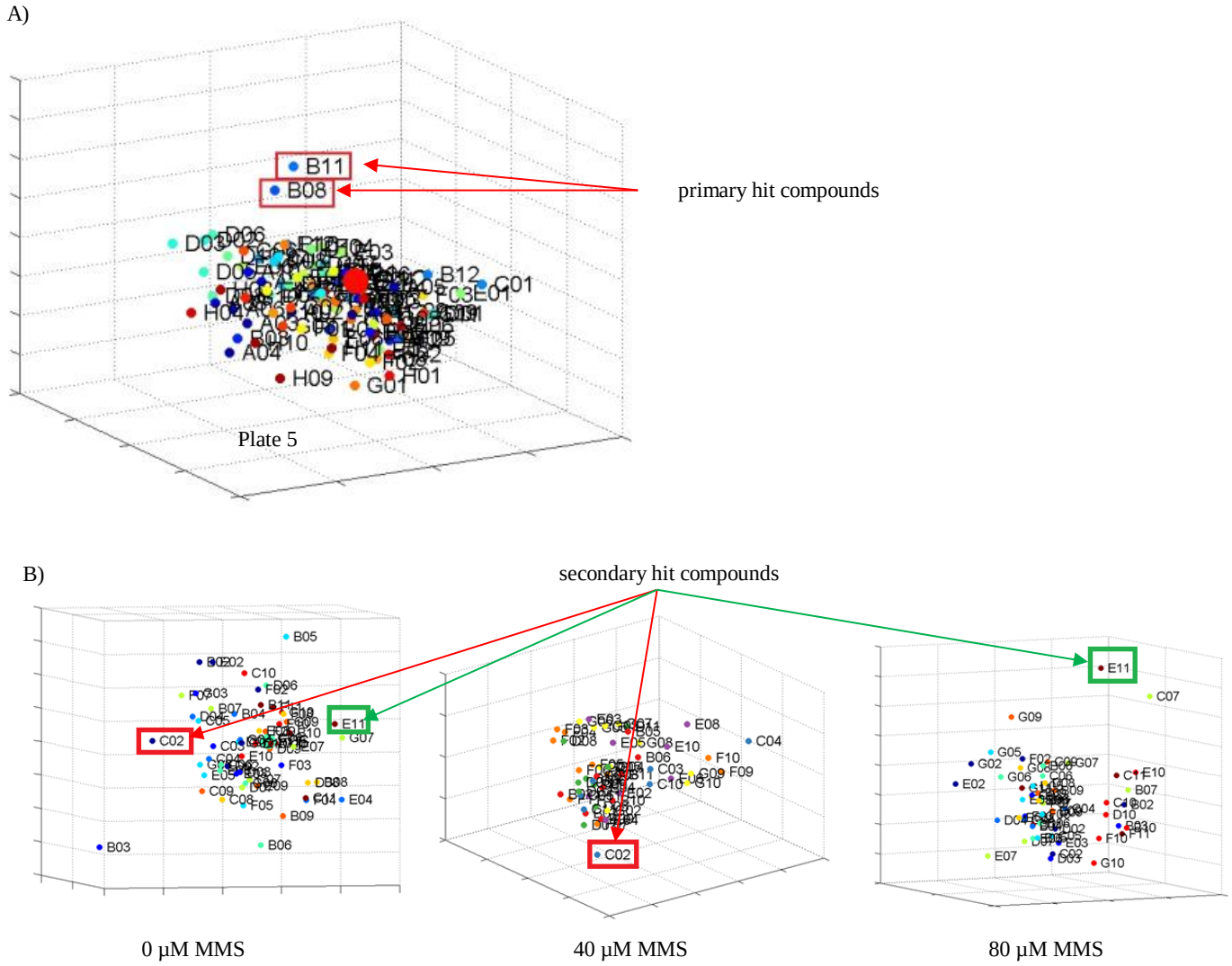

Figure 1: *Phenoripper PCA plots of the primary and secondary screens of the FDA compound library.* Cells were treated with compounds at 1 µM for 6 hours at 37˚C, fixed with cold methanol, blocked, and incubated with Alexa Fluor 488-conjugated anti–N17-S13pS16p primary antibody overnight. Plates were imaged microscopically at 20X magnification and images were analyzed for principal component analysis by Phenoripper. The points farthest away from the center of the plots were selected as primary hits. A) PCA plot of FDA compound plate 8 primary screen. B) PCA plots of a secondary screen conducted on cells pretreated with either 0, 40, or 80 µM of MMS for 20 minutes. Compounds that were hits in at least two of the three conditions were considered hits.

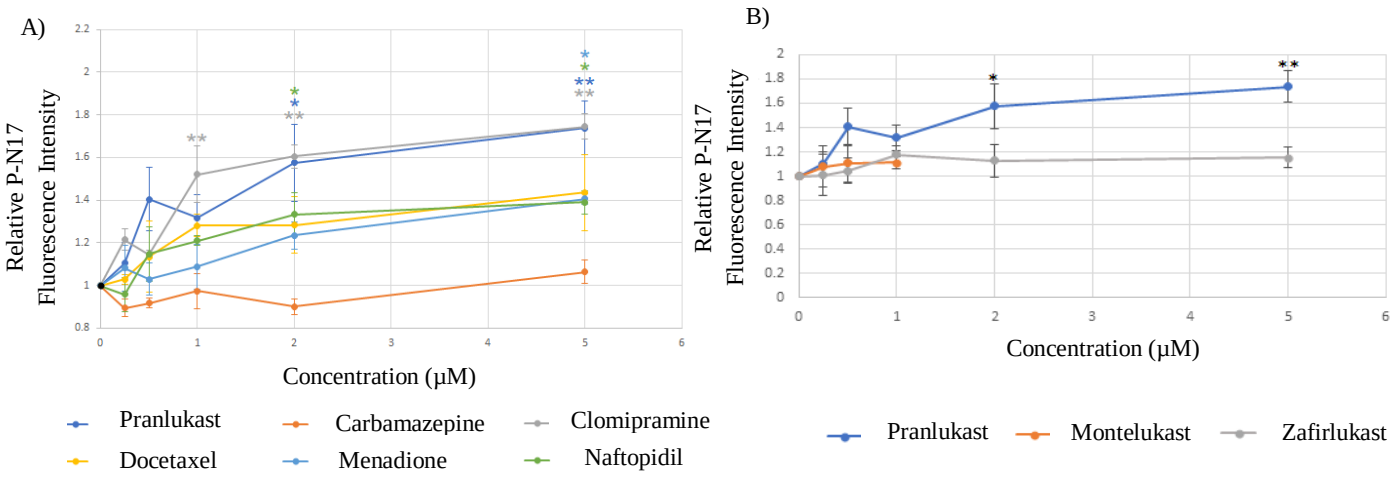

Figure 2: *Phospho-N17 dose response curves*. Cells were treated with 0.25, 0.5, 1, 2, and 5 µM for 6 hours, fixed with cold methanol, and treated with Alexa Fluor 488-conjugated anti–N17-S13pS16p primary antibody overnight. Images were acquired with the EVOS FL Auto at 20X magnification. Relative fluorescence intensity was measured using CellProfiler. N=3. **P<0.001, *P<0.05. Statistical analysis was performed using one-way ANOVA. A) Dose response curves of five final hit compounds and one non-hit compound (Carbamazepine). B) Dose response curves of cysteinyl leukotriene receptor antagonists.

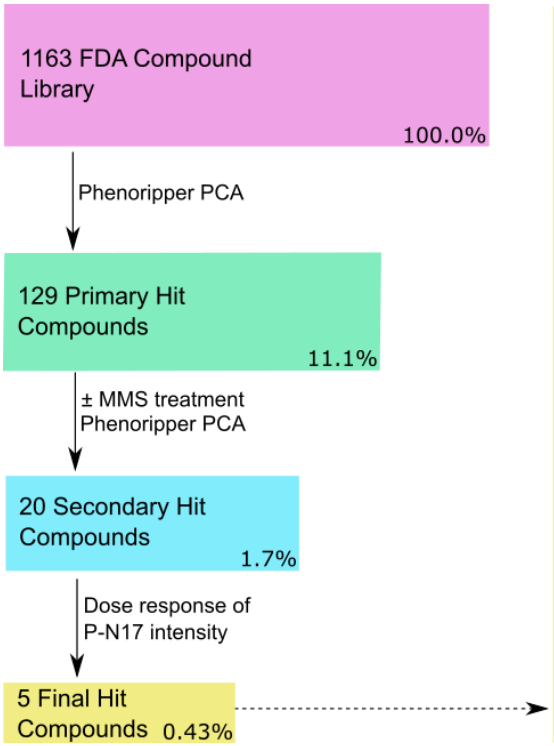

Compound	Indication	Structure
Clomipramine	Antidepressant	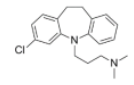
Docetaxel	Chemotherapy	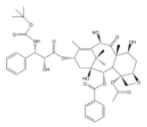
Menadione	Vitamin K supplement for animals	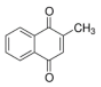
Naftopidil	Benign prostatic hyperplasia	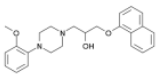
Pranlukast	Bronchospasms, asthma, allergies	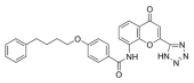

Figure 3: *Summary of the Gladiator screen and the five final hit compounds.*

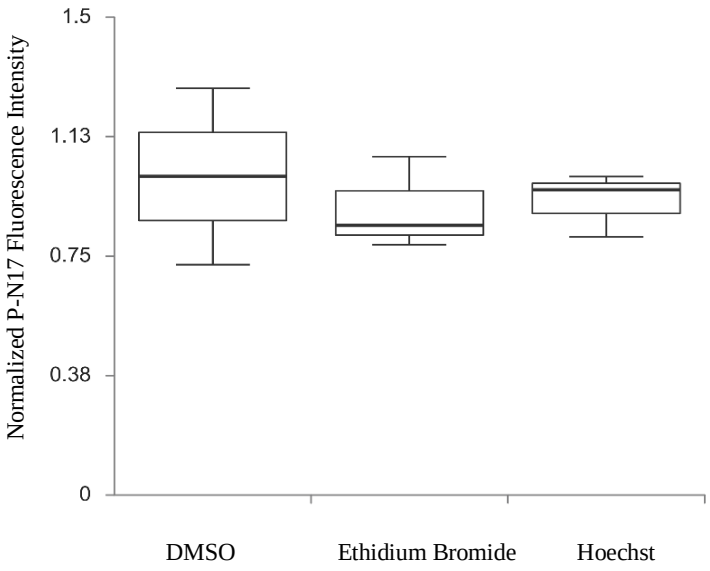

Figure 4: *Effect of DNA intercalation on phosphorylated N17.* Live cells were treated with Ethidium and Hoechst dye. Cells were treated in triplicate with 10 µg/ml ethidium bromide and Hoechst 33342 dye for 2 hours and 20 minutes respectively. The cells were then fixed with cold methanol and treated with Alexa Fluor 488-conjugated anti–N17-S13pS16p primary antibody overnight. Images were acquired with the EVOS FL Auto at 20X magnification, and relative fluorescence intensity was measured with CellProfiler. N=3.

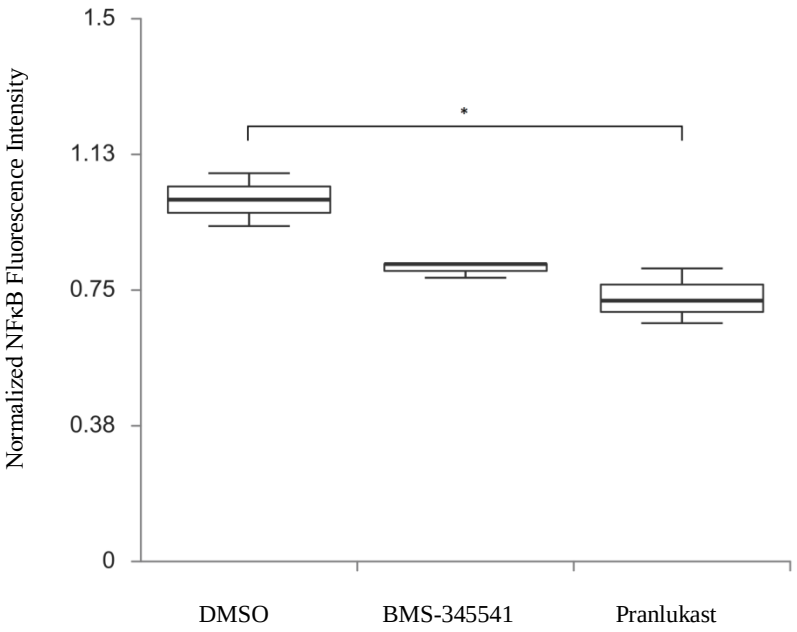

Figure 5: *Effect of Pranlukast on NFκB levels.* Cells were treated with either BMS-345541 (10μM), Pranlukast (5μM), or vehicle control for two hours, fixed in 4% PFA at room temperature, and permiabilized with 0.1% Triton X-100. Cells were then treated with an anti-NFκB p65 antibody overnight, and then with secondary antibody for 30 minutes. Images were acquired with the EVOS FL Auto at 20X magnification, and relative fluorescence intensity was measured with CellProfiler. N=3. **P<0.001, *P<0.05. Statistical analysis was performed using one-way ANOVA.

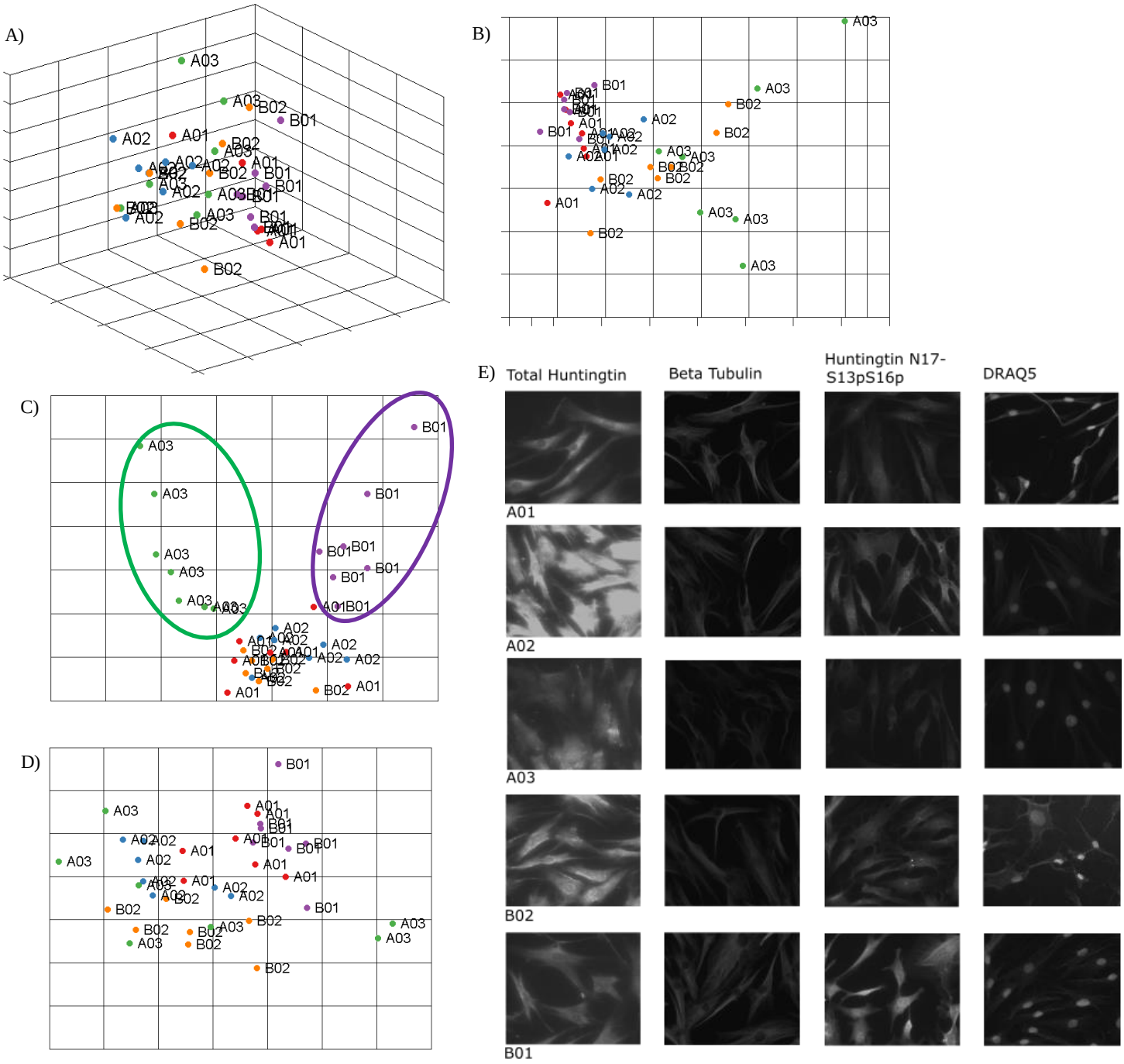

Figure 6: *Principal component analysis of PRMT5 inhibitors.* Cells were treated with DMSO (A01), SGC-2096 (A02), GSK-591 (A03), LLY-283 (B01), or LY-284 (B02) for 24 hours, fixed with methanol, and blocked. Immunofluorescence was used to visualize total huntingtin (A), beta tubulin (B), and phosphorylated N17 (C). Nuclei were stained with DRAQ5 (D). Images were acquired with the EVOS FL 2 scope and analyzed with Phenoripper software. (E) Images of cell treated with the compounds in all channels.

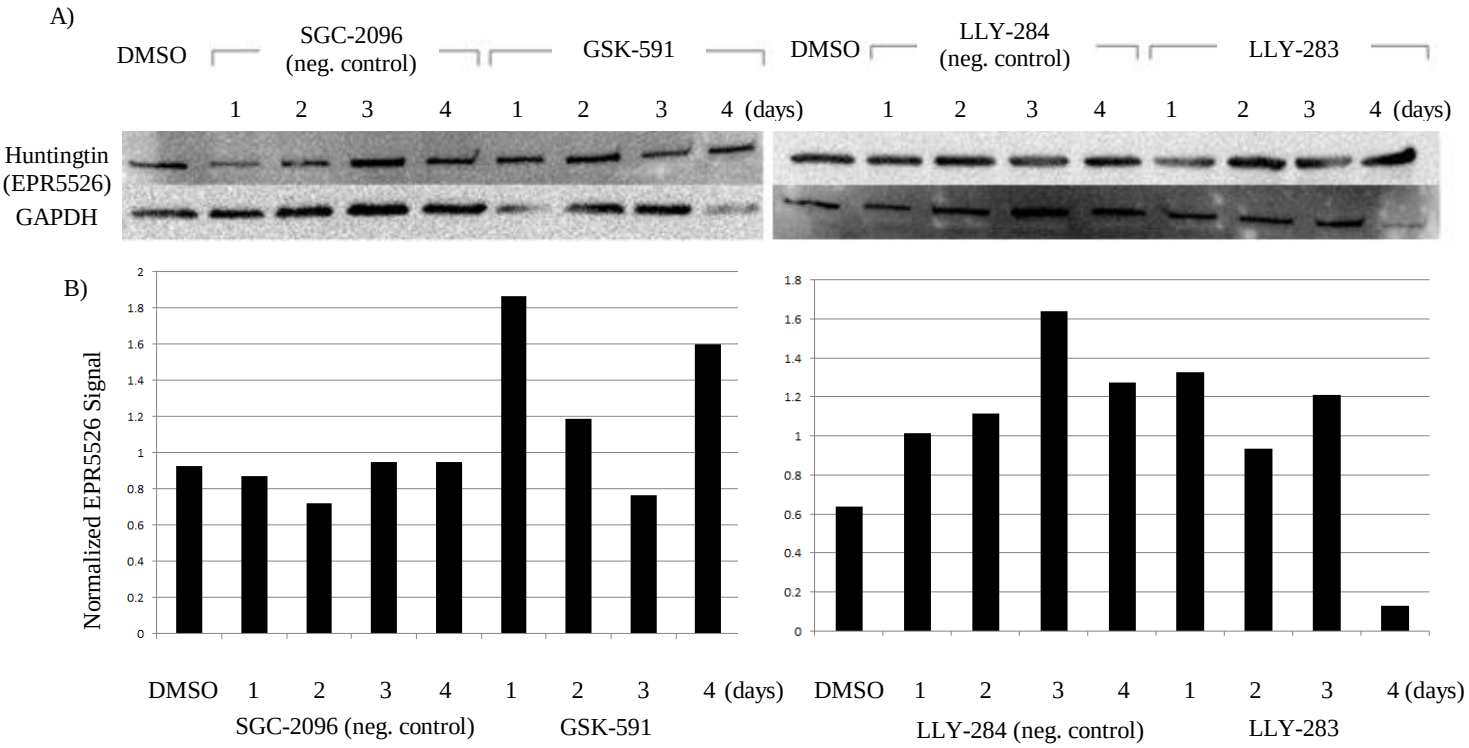

Figure 7: *Time response of huntingtin levels in cells treated with PRMT5 inhibitors.* Cells were treated with 1μM of the compounds for 1, 2, 3, or 4 days. Cells were lysed, run on an SDS-PAGE, and electroblotted onto a PVDF membrane. The EPR5526 anti-huntingtin antibody was used to treat the huntingtin bands, followed by a secondary antibody. Huntingtin was quantified and normalized to GAPDH loading control intensities using ImageJ. A) Western blots of treated cells. B) Western blot quantifications.

References

1. Huntington G. On Chorea. Medical and Surgical Reporter. Philadelphia: SW Butler; 1872.
2. Walker,F.O. (2007) Huntington's disease. *Lancet*, **369**, 218–28.
3. Roos,R.A.C. (2010) Huntington's disease: a clinical review. *Orphanet. J. Rare. Dis.*, **5**, 40.
4. Lanska,D.J., Lanska,M.J., Lavine,L. and Schoenberg,B.S. (1988) Conditions associated with Huntington's disease at death. A case-control study. *Arch. Neurol.*, **45**, 878–880.
5. Sørensen,S.A. and Fenger,K. (1992) Causes of death in patients with Huntington's disease and in unaffected first degree relatives. *J. Med. Genet.*, **29**, 911–914.
6. Vonsattel,J.-P., Myers,R.H., Stevens,T.J., Ferrante,R.J., Bird,E.D. and Richardson,E.P. (1985) Neuropathological Classification of Huntington's Disease. *J. Neuropathol. Exp. Neurol.*, **44**, 559–577.
7. The Huntington's Disease Collaborative Research Group. (1993) A novel gene containing a trinucleotide repeat that is expanded and unstable on Huntington's disease chromosomes. *Cell*, **72**, 971–983.
8. Stine,O.C., Pleasant,N., Franz,M.L., Abbott,M.H., Folstein,S.E., and Ross,C.A. (1993) Correlation between the onset age of Huntington's disease and length of the trinucleotide repeat in IT-15. *Hum. Mol. Genet*., **2**, 1547–1549.
9. Langbehn,D.R., Brinkman,R.R., Falush,D., Paulsen,J.S., and Hayden,M.R. (2004) A new model for prediction of the age of onset and penetrance for Huntington's disease based on CAG length. *Clin. Genet.* **65**, 267-277.
10. Genetic Modifiers of Huntington's Disease (GeM-HD) Consortium (2015). Identification of Genetic Factors that Modify Clinical Onset of Huntington's Disease. *Cell*. **162**, 516–526.
11. Telenius,H., Kremer,B., Goldberg,Y.P., Theilmann,J., Andrew,S.E., Zeisler,J., Adam,S., Greenberg,C., Ives,E.J. and Clarke L.A. (1994) Somatic and gonadal mosaicism of the Huntington disease gene CAG repeat in brain and sperm. *Nat. Genet.*, **6**, 409-414.
12. De Rooij,K.E., De Koning Gans,P.A., Roos,R.A., Van Ommen,G.J. and Den Dunnen,J.T. (1995) Somatic expansion of the (CAG)n repeat in Huntington disease brains. *Hum. Genet.*, **95**, 270–274.
13. Ridley,R.M., Frith,C.D., Crow,T.J. and Conneally,P.M. (1988) Anticipation in Huntington's disease is inherited through the male line but may originate in the female. *J. Med. Genet.*, **9**, 589-95.
14. Duyao,M., Ambrose,C., Myers,R., Novelletto,A., Persichetti,F., Frontali,M., Folstein,S., Ross,C., Franz,M., Abbott,M., *et al.* (1993) Trinucleotide repeat length instability and age of onset in Huntington's disease. *Nat. Genet.*, **4**, 387-92.
15. Trottier,Y., Biancalana,V. and Mandel,J.L. (1994) Instability of CAG repeats in Huntington's disease: relation to parental transmission and age of onset. *J. Med. Genet*., **5**, 377-82.
16. Ranen,N.G., Stine,O.C., Abbott,M.H., Sherr,M., Codori,A.M., Franz,M.L., Chao,N.I., Chung,A.S., Pleasant,N., Callahan,C., *et al.* (1995) Anticipation and instability of IT-15 (CAG)n repeats in parent-offspring pairs with Huntington disease. *Am. J. Hum. Genet.*, **57**, 593-602.
17. Kremer,B., Almqvist,E., Theilmann,J., Spence,N., Telenius,H., GoldbergY.P. and Hayden,M.R. (1995) Sex-dependent mechanisms for expansions and contractions of the CAG repeat on affected Huntington disease chromosomes. *Am. J. Hum. Genet.*, **57**, 343–350.
18. Wright,G.E.B., Collins,J.A., Kay,C., McDonald,C., Dolzhenko,E., Xia,Q., Bečanović,K., Drögemöller,B.I., Semaka,A., Nguyen,C.M., *at al.* (2019) Length of Uninterrupted CAG, Independent of Polyglutamine Size, Results in Increased Somatic Instability, Hastening Onset of Huntington Disease. *Am. J. Hum. Genet.*, **104**, 1116-1126.

19. Moss,D.J.H., Pardiñas,A.F., Langbehn,D., Lo,K., Leavitt,B.R., Roos,R., Durr,A. and Mead,S. (2017) Identification of genetic variants associated with Huntington's disease progression: a genomewide association study. *Lancet Neurol.*, **16**, 701–711.
20. Maiuri,T., Mocle,A.J., Hung,C.L., Xia,J., van Roon-Mom,W.M. and Truant,R. (2017) Huntingtin is a scaffolding protein in the ATM oxidative DNA damage response complex. *Hum. Mol. Genet.*, **15**, 395-406.
21. Harjes,P. and Wanker,E.E. (2003) The hunt for huntingtin function: interaction partners tell many different stories. *Trends Biochem. Sci.*, **28**, 425-33.
22. Cattaneo,E., Zuccato,C. and Tartari,M. (2005) Normal huntingtin function: an alternative approach to Huntington's disease. *Nat. Rev. Neurosci.*, **6**, 919-30.
23. Andrade,M.A. and Bork,P. (1995) HEAT repeats in the Huntington's disease protein.
Nature. Genet., **11**, 115-116.
24. Groves,M.R. and Barford,D. (1999) Topological characteristics of helical repeat proteins
Curr. Opin. Struct. Biol., **9**, 383-389.
25. Takano,H. and Gusella,J.F. (2002) The predominantly HEAT-like motif structure of huntingtin and its association and coincident nuclear entry with dorsal, an NF-kB/Rel/dorsal family transcription factor. *BMC neurosci*. **3**, 15.
26. Palidwor,G.A., Shcherbinin,S., Huska,M.R., Rasko,T., Stelzl,U., Arumughan,A., Foulle,R., Porras,P., Sanchez-Pulido,L., Wanker,E.E., *et al.* (2009) Detection of alpha-rod protein repeats using a neural network and application to huntingtin. *PLOS Comput. Biol.*, **5**, e1000304.
27. Vijayvargia,R., Epand,R., Leitner,A., Jung,T.Y., Shin,B., Jung,R., Lloret,A., Singh Atwal,R., Lee,H, Lee,J.M., *et al.* (2016) Huntingtin's spherical solenoid structure enables polyglutamine tract-dependent modulation of its structure and function. *eLife.* **5**, e11184.
28. Guo,Q., Huang,B., Cheng,J., Seefelder,M., Engler,T., Pfeifer,G., Oeckl,P., Otto,M., Moser,F., Maurer,M., *et al.* (2018) The cryoelectron microscopy structure of huntingtin. *Nature*, **555**, 117-120.
29. Atwal,R.S., Xia,J., Pinchev,D., Taylor,J., Epand,R.M. and Truant,R. (2007) Huntingtin has a membrane association signal that can modulate huntingtin aggregation, nuclear entry and
toxicity. *Hum. Mol. Genet.*, **16**, 2600-2615.
30. Kim,M.W., Chelliah,Y., Kim,S.W., Otwinowski,Z. and Bezprozvanny,I. (2009) Secondary structure of Huntingtin amino-terminal region. *Structure*. **17**, 1205-1212.
31. Michalek,M., Salnikov,E.S. and Bechinger,B. (2013) Structure and Topology of the Huntingtin 1–17 Membrane Anchor by a Combined Solution and Solid-State NMR Approach. *Biophys. J.*, **105**, 699-710.
32. DiFiglia,M., Sapp,E., Chase,K., Schwarz,C., Meloni,A., Young,C., Martin,E.,
Vonsattel,J.P., Carraway,R. And Reeves,S.A. (1995) Huntingtin is a cytoplasmic protein
Associated with vesicles in human and rat brain neurons. *Neuron*, **14**, 1075–1081.
33. De Rooij,K.E., Dorsman,J.C., Smoor,M.A., Den Dunnen,J.T. and Van Ommen,G.J. (1996) Subcellular localization of the Huntington's disease gene product in cell lines by immunofluorescence and biochemical subcellular fractionation, *Hum. Mol. Genet.*, **5**, 1093-1099.
34. Xia,J., Lee,D.H., Taylor,J., Vandelft,M. and Truant,R. (2003) Huntingtin contains a highly conserved nuclear export signal. *Hum. Mol. Genet.*, **12**, 1393-1403.
35. DiGiovanni,L.F., Mocle,A.J., Xia,J. and Truant,R. (2016) Huntingtin N17 domain is a
reactive oxygen species sensor regulating huntingtin phosphorylation and localization.
Hum. Mol. Genet., **25**, 3937-3945.
36. Atwal,R.S., Desmond,C.R., Caron,N., Maiuri,T., Xia,J., Sipione,S. and Truant,R. (2011)

Kinase inhibitors modulate huntingtin cell localization and toxicity. *Nat. Chem. Biol.*, **7**, 453–460.
37. Desmond,C.R., Atwal,R.S., Xia,J. and Truant,R. (2012) Identification of a Karyopherin β1/β2 Proline-Tyrosine Nuclear Localization Signal in Huntingtin Protein. *J. Biol. Chem.*, **287**, 39626–39633.
38. Son,S., Bowie,L.E., Maiuri,T., Hung,C.L.K, Desmond,C.R., Xia,J. and Truant,R. (2018) High-mobility group box 1 links sensing of reactive oxygen species by huntingtin to its nuclear entry. *J. Biol. Chem.*, **294**, 1915–1923.
39. Hung,C.L., Maiuri,T., Bowie,L.E., Gotesman,R., Son,S., Falcone,M., Giordano,J.V., Gillis,T., Mattis,V., Lau,T., *et al.* (2018) A patient-derived cellular model for Huntington disease reveals phenotypes at clinically relevant CAG lengths. *Mol. Biol. Cell*, **29**, 2809-2820.
40. Maiuri,T., Woloshansky,T., Xia,J. and Truant,R. (2013) The huntingtin N17 domain is a multifunctional CRM1 and Ran-dependent nuclear and cilial export signal. *Hum. Mol. Genet.*, **22**, 1383–1394.
41. Guttler,T. and Gorlich,D. (2011) Ran-dependent nuclear export mediators: a structural perspective. *EMBO J.*, **30**, 3457-3474.
42. Perutz,M.F. (1996) Glutamine repeats and inherited neurodegenerative diseases: molecular aspects. *Curr. Opin. Struct. Biol.*, **6**, 848-858.
43. Mangiarini,L., Sathasivam,K., Seller,M., Cozens,B., Harper,A., Hetherington,C., Lawton,M., Trottier,Y., Lehrach,H., Davies,S.W., *et al.* (1996) Exon 1 of the HD gene with an expanded CAG repeat is sufficient to cause a progressive neurological phenotype in transgenic mice. *Cell*, **87**, 493-506.
44. DiFiglia,M., Sapp,E., Chase,K.O., Davies,S.W., Bates,G.P., Vonsattel,J.P. and Aroninet,N. (1997) Aggregation of huntingtin in neuronal intranuclear inclusions and dystrophic neurites in brain. *Science*, **277**, 1990–1993.
45. Saudou,F., Finkbeiner,S., Devys,D. and Greenberg,M.E. (1998) Huntingtin acts in the nucleus to induce apoptosis but death does not correlate with the formation of intranuclear inclusions. *Cell*, **95**, 55-66.
46. Arrasate,M., Mitra,S., Schweitzer,E.S., Segal,M.R. and Finkbeiner,S. (2004) Inclusion body formation reduces levels of mutant huntingtin and the risk of neuronal death, *Nature*, **431**, 805-810.
47. Caron,N.S., Hung,C.L., Atwal,R.S. and Truant,R. (2014) Live cell imaging and biophotonic methods reveal two types of mutant huntingtin inclusions. *Hum. Mol. Genet.*, **23**, 2324–2338.
48. Maiuri,T., Bowie,L.E. and Truant,R. (2019) DNA Repair Signaling of Huntingtin: The Next Link Between Late-Onset Neurodegenerative Disease and Oxidative DNA Damage. *DNA Cell Biol.*, **38**, 1-6.
49. Maiuri,T., Suart, C.E., Hung,C.L.K., Graham,K.J., Barba Bazan,C.A. and Truant,R.(2019) DNA Damage Repair in Huntington's Disease and Other Neurodegenerative Diseases. *Neurotherapeutics.*, https://doi.org/10.1007/s13311-019-00768-7.
50. Mochel,F., N'Guyen,T.-M., Deelchand,D., Rinaldi,D., Valabregue,R., Wary,C., Carlier,P.G., Durr,A. and Henry,P.G. (2012) Abnormal response to cortical activation in early stages of Huntington disease. *Mov. Disord.*, **27**, 907-910.
51. Mochel,F., Durant,B., Meng,X., O'Callaghan,J., Yu,H., Brouillet,E., Wheeler,V.C., Humbert,S., Schiffmann,R. and Durr,A. (2012) Early alterations of brain cellular energy homeostasis in Huntington disease models. *J. Biol. Chem.*, **287**, 1361-1370.

52. Carmo,C., Naia,L., Lopes,C. and Rego,A.C. (2018) Mitochondrial dysfunction in Huntington's disease. *Adv. Exp. Med. Biol.*, **1049**, 59-83.
53. Gu,X., Greiner,E.R., Mishra,R., Kodali,R., Osmand,A., Finkbeiner,S., Steffan,J.S., Thompson,L.M., Wetzel,R. and Yang,X.W. (2009) Serines 13 and 16 are critical determinants of full-length human mutant huntingtin induced disease pathogenesis in HD mice. *Neuron*, **64**, 828-840.
54. Di Pardo,A., Maglione,V., Alpaugh,M., Horkey,M., Atwal,R.S., Sassone,J., Ciammola,A., Steffan,J.S., Fouad,K., Truant,R., *et al.* (2012) Ganglioside GM1 induces phosphorylation of mutant huntingtin and restores normal motor behavior in Huntington disease mice. *Proc. Natl. Acad. Sci.*, **109**, 3528-3533.
55. Truant,R., Atwal,R.S., Desmond,C., Munsie,L. and Tran,T. (2008) Huntington's Disease:
Revisiting the aggregation hypothesis in polyglutamine neurodegenerative diseases.
FEBS J., **275**, 4252–4262.
56. Caron,N.S., Desmond,C.R., Xia,J. and Truant,R. (2013) Polyglutamine domain flexibility mediates the proximity between flanking sequences in huntingtin. *Proc. Natl. Acad. Sci.*, **110**, 14610–14615.
57. Williamson,T.E., Vitalis,A., Crick,S.L. and Pappu,R.V. (2010) Modulation of polyglutamine conformations and dimer formation by the N-terminus of Huntingtin. *J. Mol. Biol.*, **396**, 1295-1309.
58. Kim,M.W., Chelliah,Y., Kim,S.W., Otwinowski,Z. and Bezprozvanny,I. (2009) Secondary Structure of Huntingtin Amino-Terminal Region. *Structure.*, **17**, 1205-1212.
59. Bowie,L.E., Maiuri,T., Alpaugh,M., Gabriel,M., Arbez,N., Galleguillos,D., Hung,C.L.K.,
PXia,J., Hertz,N.T., *et al.* (20atel,S., 18) N6-Furfuryladenine is protective in Huntington's disease models by signaling huntingtin phosphorylation. *Proc. Natl. Acad. Sci.*, **115**, E7081-E7090.
60. Barciszewski,J., Barciszewska,M.Z., Siboska,G., Rattan,S.I. and Clark,B.F. (1999) Some unusual nucleic acid bases are products of hydroxyl radical oxidation of DNA and RNA. *Mol. Biol. Rep.*, **26**, 231–238.
61. Wyszko,E., Barciszewska,M.Z., Markiewicz,M., Szymański,M., Markiewicz,W.T., Clark,B.F. and Barciszewski,J. (2003) “Action-at-a distance” of a new DNA oxidative damage product 6-furfuryl-adenine (kinetin) on template properties of modified DNA. Biochim Biophys Acta 1625:239–245.
62. Hertz,N.T., Berthet,A., Sos,M.L., Thorn,K.S., Burlingame,A.L., Nakamura,K. and Shokat,K.M. (2013) A neo-substrate that amplifies catalytic activity of Parkinson’s-disease-related kinase PINK1. *Cell*, **154**, 737–747.
63. Kordasiewicz,H.B., Stanek,L.M., Wancewicz,E.V., Mazur,C., McAlonis,M.M., Pytel,K.A., Artates,J.W., Weiss,A., Cheng,S.H., Shihabuddin,L.S., *et al.* (2012) Sustained therapeutic reversal of Huntington's disease by transient repression of huntingtin synthesis. *Neuron.*, **74**, 1031-1044.
64. Tabrizi,S.J., Leavitt,B.R., Landwehrmeyer,G.B., Wild,E.J., Saft,C., Barker,R.A., Blair,N.F., Craufurd,D., Priller,J., Rickards,H., *et al.* (2019) Targeting Huntingtin Expression in Patients with Huntington's Disease. *N. Engl. J. Med.*, **380**, 2307-2316.
65. Safety and Tolerability of WVE-120102 in Patients With Huntington’s Disease - Full Text View - ClinicalTrials.gov Available at: https://clinicaltrials.gov/ct2/show/NCT03225846?term=Wave&type=Intr&cond=Huntington+Disease&rank=1 [Accessed August 23, 2019].
66. Rajaram,S., Pavie,B., Wu,L.F. and Altschuler,S.J. (2012) PhenoRipper: Software for rapidly profiling microscopy images. *Nat. Methods*, **9**, 635–637.

67. Kamentsky,L., Jones,T.R., Fraser,A., Bray,M., Logan,D., Madden,K., Ljosa,V., Rueden,C., Harris,G.B., Eliceiri,K., *et al.* (2011). Improved structure, function, and compatibility for CellProfiler: modular high-throughput image analysis software. *Bioinformatics*, **27**, 1179–1180.
68. Lee,K.S., Kim,S.R., Park,H.S., Park,S.J., Min,K.H., Lee,K.Y., Jin,S.M. and Lee,Y.C. (2007) Cysteinyl leukotriene upregulates IL-11 expression in allergic airway disease of mice. *J. Allergy Clin. Immunol.*, **119**, 41-49.
69. Ichiyama,T., Hasegawa,S., Umeda,M., Terai,K., Matsubara,T. and Furukawa,S. (2003) Pranlukast inhibits NF-kappa B activation in human monocytes/macrophages and T cells. *Clin. Exp. Allergy*, **33**, 802-807.
70. Maeba,S., Ichiyama,T., Ueno,Y., Makata,H., Matsubara,T. and Furukawa,S. (2005) Effect of montelukast on nuclear factor κB activation and proinflammatory molecules. *Ann. Allergy Asthma Immunol.*, **94**, 670–674.
71. Tintinger,G.R., Feldman,C., Theron,A.J. and Anderson,R. (2010) Montelukast: More than a Cysteinyl Leukotriene Receptor Antagonist? *Sci. World J.*, **10**, 2403-2413.
72. El-Demerdash,E. and Mohamadin,A.M. (2004) Does oxidative stress contribute in tricyclic antidepressants-induced cardiotoxicity? *Toxicol Lett.*, **152**, 159-166.
73. Varbiro,G., Veres,B., Gallyas,F.Jr. and Sumegi,B. (2001) Direct effect of Taxol on free radical formation and mitochondrial permeability transition. *Free Radic. Biol. Med.*, **31**, 548-558.
74. Halilovic,A., Schmedt,T., Benischke,A.S., Hamill,C., Chen,Y., Santos,J.H. and Jurkunas,U.V. (2016) Menadione-Induced DNA Damage Leads to Mitochondrial Dysfunction and Fragmentation During Rosette Formation in Fuchs Endothelial Corneal Dystrophy. *Antioxid. Redox Signal.*, **24**, 1072-1083.
75. Loor,G., Kondapalli,J., Schriewer,J.M., Chandel,N.S., Vanden Hoek,T.L. and Schumacker,P.T. (2010) Menadione triggers cell death through ROS-dependent mechanisms involving PARP activation without requiring apoptosis. *Free Radic. Biol. Med.*, **49**, 1925-1936.
76. Morgan,M.J. and Liu Z. (2011) Crosstalk of reactive oxygen species and NF-κB signaling. *Cell Res.*, **21**, 103–115.
77. Mattson,M.P., Goodman,Y., Luo,H., Fu,W. and Furukawa,K. (1998) Activation of NF-κB protects hippocampal neurons against oxidative stress-induced apoptosis: Evidence for induction of manganese superoxide dismutase and suppression of peroxynitrite production and protein tyrosine nitration. *J Neurosci Res.*, **49**, 681-697.
78. Mattson,M.P. and Meffert,M.K. (2006) Roles for NF-κB in nerve cell survival, plasticity, and disease. *Cell Death Differ.*, **13**, 852–860.
79. Yu,Z., Zhou,D., Cheng,G. and Mattson,M.P. (2000) Neuroprotective Role for the p50 Subunit of NF-gB in an Experimental Model of Huntington's Disease. *J. Mol. Neurosci.*, **15**, 31–44.
80. Yu,Z., Zhou,D., Bruce-Keller,A.J., Kindy,M.S. and Mattson,M.P. (1999) Lack of the p50 Subunit of Nuclear Factor-kB Increases the Vulnerability of Hippocampal Neurons to Excitotoxic Injury. *J. Neurosci.*, **19**, 8856–8865.
81. Karkhanis,V., Hu,Y.J., Baiocchi,R.A., Imbalzano,A.N. and Sif,S. (2011) Versatility of PRMT5-induced methylation in growth control and development. *Trends Biochem Sci.*, **36**, 633-641.
82. Bonday,Z.Q., Cortez,G.S., Grogan,M.J., Antonysamy,S., Weichert,K., Bocchinfuso,W.P., Li, F., Kennedy,S., Li,B., Mader,M.M., *et al.* (2018) LLY-283, a Potent and Selective Inhibitor of Arginine Methyltransferase 5, PRMT5, with Antitumor Activity. *ACS Med. Chem. Lett.*, **9**, 612-617.

83. Chan-Penebre,E., Kuplast,K.G., Majer,C.R., Boriack-Sjodin,P.A., Wigle,T.J., Johnston,L.D., Rioux,N., Munchhof,M.J., Jin,L., Jacques,S.L., *et al.* (2015) A selective inhibitor of PRMT5 with in vivo and in vitro potency in MCL models. *Nat. Chem. Biol.*, **11**, 432−437.